ARTICLE

Sol–Gel-Derived Epitaxial Nanocomposite Thin Films with Large Sharp Magnetoelectric Effect

Bin Liu, Tao Sun, Jiaqing He, and Vinayak P. Dravid*

Department of Materials Science and Engineering, International Institute of Nanotechnology, Northwestern University, Evanston, Illinois 60208, United States

ABSTRACT Nanostructures of multiferroic materials have drawn increasing interest due to the enhanced magnetoelectric coupling and potential for next-generation multifunctional devices. Most of these structures are typically prepared by thin film evaporation approaches. Herein, however, we report a novel sol–gel-based process to synthesize epitaxial $BaTiO_3$–$CoFe_2O_4$ nanocomposite thin films *via* phase separation and enhanced heterogeneous nucleation. The magnetoelectric coupling effect is investigated by examining the temperature-dependent magnetization of the composite film, which manifests as a sharp and significant drop (>50%) of the magnetization at the vicinity of a $BaTiO_3$ ferroelectric phase transition. We propose that the phase transition in $BaTiO_3$ is mediated by the tensile strain due to intimate coupling to $CoFe_2O_4$ phase, which has rarely been reported before. The significant coupling effect is attributed to the small substrate clamping, and the large areal distribution of intimate heteroepitaxial interfaces between the three-dimensionally distributed ferroelectric and magnetic nanostructured phases.

KEYWORDS: multiferroic · nanocomposite · epitaxy · magnetoelectric · sol–gel

Multiferroic magnetoelectric (ME) materials exhibit simultaneous ferroelectric (FE) and (anti)ferro- or ferrimagnetic (FM) properties, as well as effective coupling between the dual order parameters. Although the work on ME materials can be traced back to early studies in the 1960s,[1] the recent revival of the research interest has resulted in remarkable progress in the growth, characterization, and application of both single-phase materials and heterostructures. This renewed interest in ME is driven by both theoretical advances in coupled phenomena and technological prospects in novel devices.[2–4] However, due to scarcity and much weaker room-temperature ME coupling in single phase materials,[2] more efforts in application have been directed toward two-phase heterostructures because of their greater design flexibility and multifunctionality.[3]

The indirect strain-induced ME effect between the FE and FM phases provides a promising alternative strategy to enhance the coupled phenomena and resultant properties. In the meanwhile, nanostructured FE–FM composites have been explored in film-on-substrate geometry.[3] The intimate contact between the two phases and the reduced substrate clamping are crucial for achieving a large ME effect.[4] The pioneering work by Zheng *et al.*,[5] which introduced self-assembled epitaxial vertical heterostructures with FM nanopillars in an FE matrix, noted as 1–3 nanostructures,[6] has triggered widespread research activities.[7–11] Hitherto, high-quality epitaxial multiferroic nanocomposite thin films have been grown almost exclusively by high vacuum thin film deposition methods, such as pulse laser deposition (PLD). Sol–gel processing, on the other hand, exhibits many processing advantages such as ease of setup, flexible control of the phase constituents and possible dopants, cost-effectiveness, and large-area coverage.[12] As a result, it has been extensively applied to fabricate various functional thin films, including nonvolatile ferroelectric memories[13] and nanocomposite superconductor films,[14] among others. Although ME composite thin films have been prepared by sol–gel-based methods,[15–17] crack-free thin films with good epitaxy are still precluded by the challenges in controlling the complicated chemical reactions in sol precursors and the general lack of control over nucleation/growth behavior in the subsequent pyrolysis and annealing.

Epitaxy, implying the registration between the substrate and thin film crystals, is generally desirable for most functional materials and applications because of the high sensitivity to strain of the electronic and magnetic properties.[18–20] In ME nanocomposite thin films, as the key for coupling effect, the elastic interaction between FE

*Address correspondence to v-dravid@northwestern.edu.

Received for review August 8, 2010 and accepted October 13, 2010.

Published online October 28, 2010. 10.1021/nn101952q

and FM phases is expected to greatly enhance when they are grown together epitaxially or with intimate contact, in general, in order to transfer strain across the interfaces.[5] However, the ME films fabricated typically using conventional sol−gel approaches are polycrystalline in nature, often containing randomly oriented grains, rendering such systems much less competitive compared to those deposited by vapor-phase growth methods. Another open question associated with ME composite films is that large sharp ME effects have only been reported hitherto for the systems as FM films epitaxially grown on FE single crystal substrates, in which the discontinuous jump of the magnetization of the films occurs when the substrates go through phase transitions or when they are being switched by an external electric field.[21−24] However, the high cost of the substrates, limited geometric variations, high drive voltage, and catastrophic failure in this type of horizontal heterostructures still remain as the bottleneck for practical applications.[22]

Herein, we report, for the first time, the fabrication of crack-free epitaxially connected ME nanocomposite thin films on normal commensurate single crystal substrates using a simple sol−gel approach, which exhibit a large and sharp ME effect in the temperature-dependent magnetization measurements. The prototypical $BaTiO_3$ (BTO) is selected as the room-temperature lead-free ferroelectric phase, while $CoFe_2O_4$ (CFO) as the ferrimagnetic phase for its large magnetostriction ($\lambda \approx -10^{-4}$) coefficient and high Curie temperature ($T_c \approx 520$ °C), deposited on (001) $SrTiO_3$ (STO) single crystal substrates.

RESULTS AND DISCUSSION

The sol−gel precursors for the growth of BTO−CFO nanocomposite films were prepared by mixing together appropriate amounts of individual BTO and CFO sols, with ethylene glycol and methoxyethanol as the solvent, and diethanolamine as the complexing agent (see Methods). The solubility and stability of the complex sols with multiple metal agents have been the challenge for sol−gel based methods. To avoid the usage of the reactive barium metal and the rigorous condition of the nonaqueous environment,[25] ethylene glycol was chosen as the solvent to dissolve highly concentrated barium acetate. On the other hand, enough amount of diethanolamine was added, as it is critical for stabilizing the complex sol containing various metal cations with water residue. As-prepared sol can be stored at room temperature in air for several months. The precursor is then spin-coated onto STO single crystal substrates at 2000 rpm for 60 s. After baking at 150 °C for 2 min, the films are fast heated to 1000 °C in air and annealed for 30 min to accomplish the self-assembly of two phases and epitaxial growth of nanocomposite thin films. Cyclic coating and annealing offer

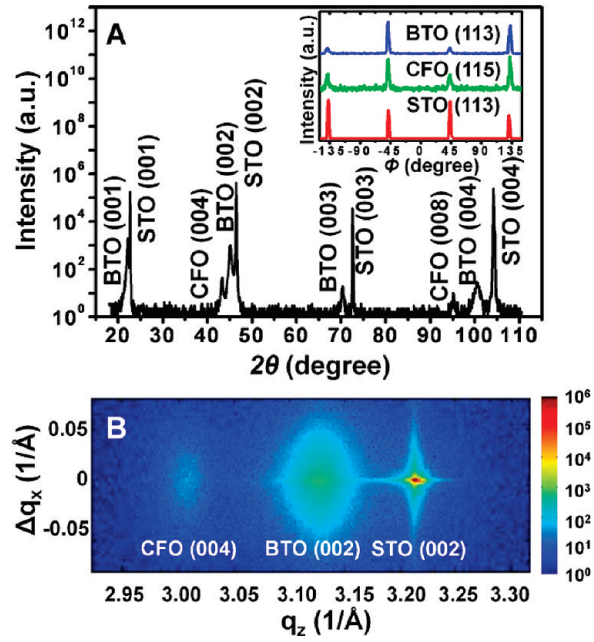

Figure 1. (A) Symmetric X-ray diffraction showing epitaxial growth of the CFO-BTO thin film on (001) STO substrate. The Φ-scan of BTO (113), CFO (115), and STO (113) atomic planes are shown in the inset, indicating the in-plane orientation of the film. (B) Reciprocal space map of STO (002), BTO (002), and CFO (004) diffraction peaks.

the desired thickness of films from 100 to 300 nm and also help minimize shrinkage stresses and cracking.

An X-ray diffraction (XRD) θ−2θ scan (Figure 1A) reveals a high degree of out-of-plane crystallographic orientation of a 100-nm-thick composite thin film with separated pure BTO and CFO phases, as all the diffraction peaks can be assigned to the (00*l*) atomic planes of the substrate STO, spinel CFO, and perovskite BTO. The in-plane orientation was investigated by Φ-scan of the film. The reflections of STO (113), BTO (113), and CFO (115) (inset in Figure 1A) all exhibit 4-fold symmetry, which indicates a cube-on-cube epitaxial relationship of both CFO and BTO phases, on the STO substrate. The reciprocal space map around BTO (002) (Figure 1B) again confirms the heteroepitaxy of the nanocomposite film, and the orientational variation of the mosaic blocks (degree of epitaxy) can also be examined by evaluating the elongation of the diffraction spots along the Δq_x direction. Direct rocking curve measurements (Supporting Information Figure S1) show an average full-width-at-half-maximum (FWHM) of 0.4° for BTO (002) and 0.8° for CFO (004), indicating good quality of epitaxy, comparable to those obtained for composite films deposited by laser molecular beam epitaxy[26] and PLD[27] on STO substrates. On the basis of angle position of XRD peaks, the lattice parameters of two phases at room temperature were determined (±0.0005 nm) to be: $a = b = 0.399$ nm, $c = 0.400$ nm for BTO; and $a = b = 0.839$ nm, $c = 0.837$ nm for CFO, which indicates that CFO has a compressive out-of-plane strain of 0.2%. It is worth pointing out that because the BTO grains

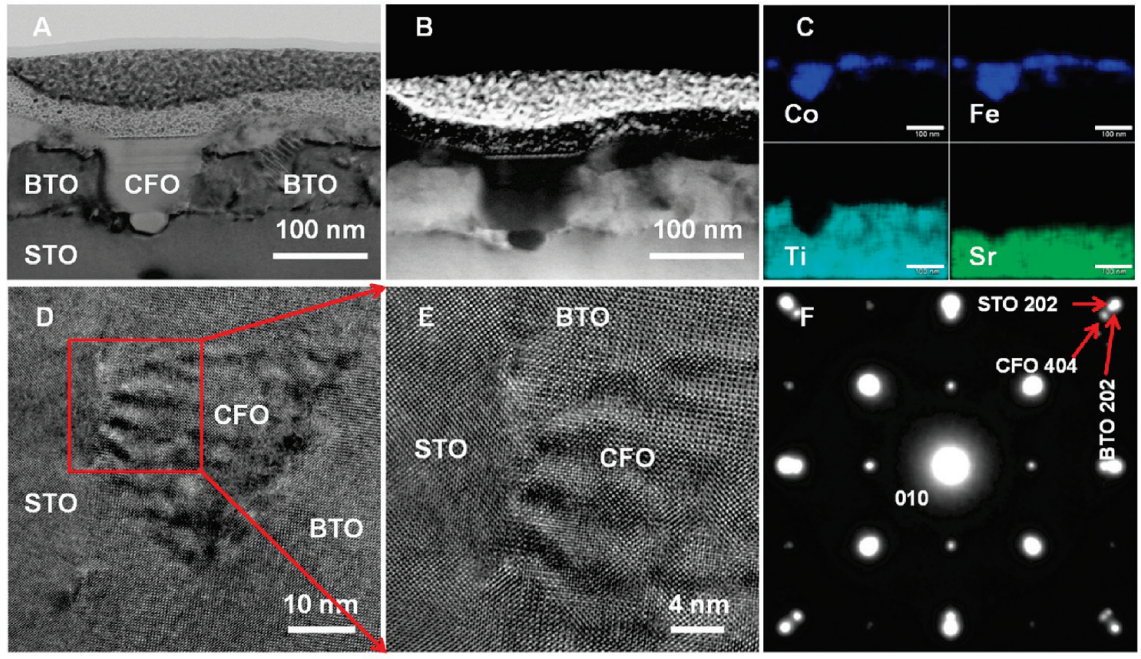

Figure 2. (A) Cross-sectional bright-field TEM image of the BTO−CFO thin film on STO substrate, and (B) corresponding STEM Z-contrast image, and (C) EDS element mapping showing the phase separation of BTO and CFO, as well as the 3D stacking of the nanoblocks. Scale bar width is 100 nm. (D) Cross-sectional high resolution TEM image of one CFO particulate embedded in BTO, and (E) high resolution TEM image of the enlarged area at the interfaces, indicating the heteroepitaxial relationship between three phases. (F) Selected-area electron diffraction pattern demonstrating both in-plane and out-of-plane epitaxy.

have epitaxial interfaces with both the substrate and adjacent CFO grains, each of them is possibly exerted with either compressive or tensile stress or both. Therefore, localized structures (and polarization domains) are likely to be diverse and complex.[28]

The transmission electron microscopy (TEM) and energy dispersive X-ray spectroscopy (EDS) study resolved the self-assembled nanocomposite structures. Figure 2 panels A, B, and C show a cross-sectional bright-field TEM image, a corresponding scanning TEM Z-contrast image, and the EDS elemental mapping of the BTO−CFO nanocomposite thin film, respectively. It can be observed that the BTO and CFO phases are well separated to form closely stacked nanoscale blocks. Moreover, some CFO particulates with 10- to 20-nm diameter are also found to be embedded in BTO phases. Figure 2 panels D and E show the cross-sectional high-resolution TEM images of the film and the enlarged area at the interfaces, which clearly reveal the commensurate epitaxial relationship among BTO, CFO, and the STO substrate. With the electron diffraction pattern (Figure 2F) in cross-sectional geometry, the epitaxial relationship can be resolved as: $(001)_{STO}//(001)_{BTO}//(001)_{CFO}$, and $[101]_{STO}//[101]_{BTO}//[101]_{CFO}$. The surface morphology of the film was examined using scanning electron microscopy (SEM) and atomic force microscopy (AFM). A faceted chessboard-type surface structure was observed with a surface roughness in the nanometer range (Supporting Information Figure S2). The observed surface roughness of the epitaxial two-phase composite thin films is likely due to the notable lattice mismatch between two phases.[29]

The self-assembly and epitaxial growth of the crack-free nanocomposite thin films from sol−gel precursors can be understood from thermodynamics and kinetics. First, as shown in the phase diagram of the pseudoquinary system Co−Fe−Ba−Ti−O,[30] the mutual solid solubility between BTO and CFO phases is very low, which is an important condition for phase separation. Meanwhile, the energy barrier for heterogeneous nucleation is always smaller than that for homogeneous nucleation, but the difference is normally so small that the external energy (*i.e.*, thermal annealing) can overcome both of them, resulting in the occurrence of two types of nucleation simultaneously.[31] Therefore, the effective strategy is to enlarge the energy barrier difference, which favors the epitaxial growth. In our experiment, several factors were considered in order to enhance heterogeneous nucleation: (1) Substrate: Given that both perovskite (BTO and STO) and spinel (CFO) structures are face-centered cubic system with octahedral oxygen coordination, and the lattice mismatch in the system is smaller than 8% (Supporting Information S3), this structural similarity is expected to lower the energy barrier for heterogeneous nucleation. (2) Multistep processing: The film was fabricated *via* cyclic deposition, that is, each layer was deposited and annealed before coating the subsequent layer. In this way, the fully crystallized film serves as preferential

heterogeneous nucleation sites (also known as seed layer) for the next layer. (3) Rapid heating: After baking, the film was directly inserted into a preheated furnace for annealing. Such a handling behaves as the rapid thermal annealing process, which forces crystallization of the film to happen at a relatively higher temperature. Since the driving force ΔG_v decreases with temperature, the delay of nucleation effectively enlarge the difference between the energy barriers of two nucleation events. (4) Sol−gel chemistry. The polymerization of the sol precursor adjusted by adding diethanolamine and the high decomposition temperature (~550 °C) (Supporting Information S4) also postpones the crystallization to higher temperatures.[31,32]

The ferroelectric and magnetic properties of the epitaxial BTO−CFO nanocomposite thin films were studied to evaluate the nature and extent of ME coupling. The electronic polarization (**P**) *versus* electric field (**E**) measurements were performed for the BTO−CFO film on Nb-doped STO substrate. The **P**−**E** hysteresis loop (Supporting Information S5) provides the clear evidence for the ferroelectric behavior of the composite film. Superconducting quantum interference device magnetometer (SQUID) was employed to probe the magnetic properties of the films. Figure 4A shows the magnetization (normalized to the volume fraction of CFO of ~50%) *versus* magnetic field (**M**−**H**) hysteresis loops obtained from the BTO−CFO film on STO substrate at room temperature, with the magnetic field perpendicular and parallel to the substrate surface, respectively. The saturation magnetization ($\mathbf{M}_s$) of the sample was measured to be ~370 emu/cm^3, comparable to the reference data,[5,33] indicating the high structural quality of the CFO phase. The similarity between the in-plane and out-of-plane **M**−**H** loops strongly suggests three-dimensionally distributed nanoparticulate heterostructure of the film, which is in contrast to the highly anisotropic nanopillar geometry prepared by PLD method.[5] The nanocomposite film has a small coercive field ($\mathbf{H}_c$) of ~650 Oe (better viewed in the insets of Figure 3A). Generally, $\mathbf{H}_c$ of CFO reaches the maximum value around 2 kOe when the particulate size is around a critical diameter (D_s) of 70 nm.[33] If smaller than D_s, the CFO grains become single domain, and magnetocrystalline anisotropy dominates the reversal process.[34] The TEM observations showed a relatively broad size distribution of CFO grains, ranging from 10 to 100 nm. However, most of the grains have the size either much smaller or larger than D_s. In this scenario, both thermal agitation and domain wall motion contribute to the small $\mathbf{H}_c$ observed from our film. It should be underscored here that both low coercivity and large magnetostriction of the FM phase can potentially enhance the ME coupling effect.[29,35]

The ME coupling effect was further investigated by examining the change of magnetization with temperature. Figure 4B shows the magnetization of the film

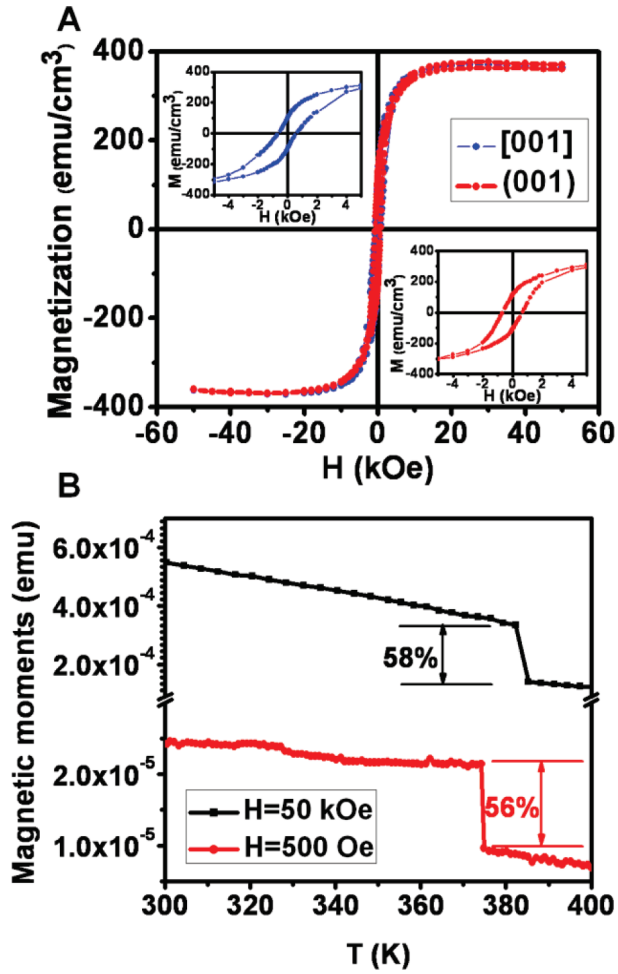

Figure 3. (A) Out-of-plane (blue) and in-plane (red) magnetic hysteresis loops at room temperature showing the isotropic magnetic property of the epitaxial CFO−BTO nanocomposite thin film. The closer looks of the loops at low field region are shown in the insets, indicating the small coercive fields of the film. (B) Magnetization as a function of temperature with the in-plane magnetic field at H = 50 kOe (black) and H = 500 Oe (red), respectively. Giant and sharp drops of the magnetization in both cases are clearly revealed.

while heating from room temperature to 400 K, measured by SQUID with in-plane magnetic field of 500 Oe and 50 kOe, respectively. Discontinuous drop of the magnetization (>50% change in the magnetization) was detected in both cases. It can also be observed that these abrupt changes occur at lower temperatures (~373 K when **H** = 500 Oe, and ~382 K when **H** = 50 kOe) than the cubic-to-tetragonal phase transition of bulk BTO (Curie temperature, $T_c \approx 398$ K).

It has been extensively reported that the phase transition of BTO in thin film or particulate forms can be highly affected by the grain size and local strain condition; however, there is still much controversy over both the phenomenon and associated mechanism(s).[36−39] For the shift of T_c, on one hand, some theoretical[40] and experimental evidence[36] indicate that the elastic strain in epitaxial BTO thin films, no matter tensile or compressive, can lead to a dramatic increase of T_c. On the other hand, some study based on Landau−Devonshire phe-

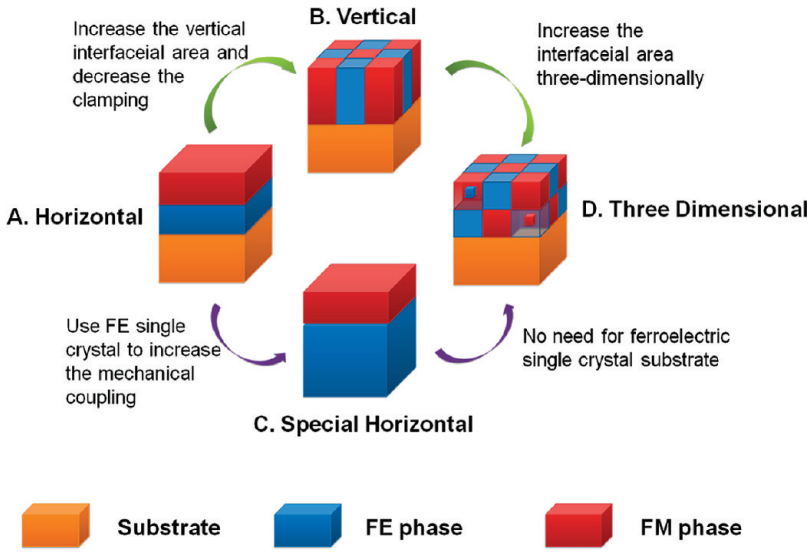

Figure 4. Schemes of the possible heterostructures and the mechanisms to increase the ME effect. (A) Horizontal heterostructure with alternating FE and FM layers. Only horizontal interfaces exist and tremendous clamping of the underlying substrate prohibits large ME effect. (B) Vertical heterostructure with pillars of FM and/or FE phases. The horizontal clamping is decreased and vertical interfacial area is large. (C) Special horizontal heterostructure. Use bulk FE single crystal as the substrate to enhance the mechanical coupling. (D) Three-dimensional heterostructure. Increase the interfacial area three-dimensionally. Blocks of both phases are stacked together and some particulates of one phase are embedded in the other phases.

nomenological theory predicts the existence of new phases (r-phase and aa-phase) with first-order transition at lower temperature in epitaxial BTO thin films under small tensile strain (<1%).[40] In regards to the sharpness of transition, it was observed that the BTO thin films and nanocrystalline ceramics often show a more diffuse phase transition compared to their bulk counterparts. Some argue that this is due to the intrinsic size effect and the thermal agitation,[37] while others suggest that the inhomogeneous effects including composition inhomogeneity, or nonuniform external fields owing to the asymmetric electrodes[41] may be responsible to diffuse transition. Furthermore, some recent results have shown that thin freestanding BTO single-crystalline film with the thickness down to ~75 nm still maintains bulk-like sharp transitions.[42,43]

In the sol−gel derived BTO−CFO nanocomposite thin films shown here, the larger lattice of CFO can induce tensile strain in BTO, which is often partially relaxed by the dislocations at the interfaces and has a relatively small value as inferred from TEM and XRD analysis. With the applied magnetic field, the magnetostrictive strain can be estimated as $e = {}^3/_2\lambda_s[(\mathbf{M}/\mathbf{M}_s)^2 - {}^1/_3]$,[33] where λ_s is the saturation magnetostriction coefficient and $\boldsymbol{M}$ and $\boldsymbol{M}_s$ are magnetization and saturated magnetization, respectively. With the **M**−**H** hysteresis, we can estimate the magnetostrictive strains of CFO under different applied fields: e(500 Oe) = $-0.06\lambda_s \approx 0$; e(50 kOe) = $\lambda_s \approx -260$ ppm. Thus, the CFO-induced tensile strain in BTO at high magnetic field is decreased due to the negative magnetostricitve strain in CFO. Due to the negative slope in the misfit-temperature phase transition line between r phase and aa phase predicted by reference,[19] the phase transition temperature of BTO at **H** = 50 kOe is larger than that at **H** = 500 Oe. In the meanwhile, the in-plane lattice parameter of BTO increases during the phase transition. This increase can be coupled to the CFO phase and would induce a decrease of magnetization due to its negative magnetostriction coefficient. However, it should be noted that the crystal structure and the strain condition of FE and FM phases in such three-dimensional (3D) nanocomposite thin films is likely to be more complex than expected, and additional experimental and theoretical work is certainly required for improved understanding.

To substantiate the unique advantages of the epitaxial BTO−CFO nanocomposite thin films, the well-studied conventional geometries of FE−FM systems as well as their comparison with our 3D heteroepitaxial ME architecture are summarized in Figure 4. The horizontal heterostructure (Scheme A) refers to those multilayers films as thin layers of FE and FM phases deposited alternatively on substrates. This is a simple geometry and easy to fabricate, so it is the earliest model for the film-type ME system and still extensively investigated currently. However, the film with this geometry is severely clamped by the substrate, which constrains the structure change of the FE and FM phases in response to external conditions, such as magnetic/electric fields and temperature, among others. To overcome this drawback, two other models are proposed: vertical (Scheme B) and special horizontal (Scheme C) heterostructures. The vertical heterostructure describes the pillar-in-matrix geometry, in which there are more interfaces between FE and FM phases while the substrate clamping effect is effectively reduced.[5] Special horizontal heterostructure improves the ME property through another way. In this model, FE single crystals are used as the substrate for deposition of FM thin films. Even though a large ME effect has been observed from the samples with CFO films epitaxially grown on single-crystalline BTO substrates, the high cost of the FE substrate and limited variations make this geometry less attractive. The sol−gel derived BTO−CFO nanocomposite films (Scheme D) studied here are a natural evolution of the vertical geometry. Since both phases exist as nanoparticulates in this architecture, interfacial area between them is further increased, so that the ME effect is larger (>50% in 1 K step, compared to ~5% in 30 K step in 1−3 geometry[5]). Compared to special horizontal model, besides the advantage of using traditional substrates, the ME coupling in the present 3D heterostructures is still remarkable. For example, Chopdekar *et al.*[44] reported ~20% change of

the magnetization of epitaxial CFO thin film in a 1 K step when the underlying BTO single crystal goes through the phase transition from rhombohedral to monoclinic at 185 K.

CONCLUSIONS

3D heteroepitaxial BTO−CFO nanocomposite thin films were grown on STO substrates using a simple sol−gel phase separation approach, which can be applied to other composite systems. A notably large and sharp magnetoelectric coupling was observed, which makes this system a promising candidate for high performance devices such as sensors and information storage media. The shift of the phase transition at lower temperatures and the unusual sharpness are explained with a new phase transition in BTO predicted by the phenomenological Landau−Devonshire theory of strained thin film ferroelectrics. We believe that the epitaxial nanocomposite ME thin films developed here can serve as another excellent test-bed, in addition to nanopillar geometry, for studying the strain and size effects on the nanostructured ferroelectric materials, as well as the coupling behavior of magnetoelectric systems.

METHODS

Samples. The BTO−CFO sols were prepared as follows. BTO and CFO sols were prepared separately first. The method to prepare 0.2 mol/L CFO sol can be found elsewhere.[45] To prepare ~0.2 mol/L BTO sol, 2.04 g of barium acetate was dissolved in the solvent with 35 mL of ethylene glycol and 3.2 mL of diethanolamine at 60 °C. A 3.89 g portion of titanium diisopropoxide bis(acetylacetonate) (75 wt % solution in propanol) was then added dropwise into the solution. Stir the solution at 70 °C until it becomes clean and transparent, which takes less than 3 h. Then 0.2 mol/L CFO sol and 0.2 mol/L BTO were mixed with equivalent volume at 70 °C and stirred for 1 h. The as-prepared BTO−CFO sol was dark red and stable at room temperature for more than three months. To prepare the thin film, the BTO−CFO sol was spin-coated on the STO substrates at 2000 rpm for 1 min, followed by 2 min of baking at 150 °C and fast annealing at 1000 °C for 30 min. Repeat the previous process for four times to obtain the film with the thickness of 100 nm.

Characterization. X-ray diffraction measurments were taken with Rigaku ATX-G thin-film diffraction workstation. The TEM sample was prepared by focused ion beam milling with FEI Helios NanoLab Dual Beam SEM/FIB. Bright field TEM and scanning TEM images and high resolution TEM were taken with JEOL JEM-2100F FAST TEM at the accelerating voltage of 200 keV. EDS element mapping was taken with Hitachi HD-2300 FE-STEM at the accelerating voltage of 120 keV. Ferroelectric measurements were performed using a Radiant Technologies RT66A system. Magnetic properties were measured with a Quantum Design Magnetometer (MPMS5) with the magnetic field aligned parallel or normal to the thin films.

Acknowledgment. This work was supported by US DOE-BES (DE-FG02-07ER46444). The TEM, SEM, and AFM studies were performed in EPIC and NIFTI facility of NU*ANCE* center at Northwestern University. NU*ANCE* center was supported by NSF-NSEC, NSF-MRSEC, Keck Foundation, the State of Illinois, and Northwestern University. This work also made use of the J. B. Cohen X-ray Diffraction facility supported by the MRSEC program of the National Science Foundation (DMR-0520513) at the Materials Research Center at Northwestern University.

Supporting Information Available: Rocking curves of BTO (002) and CFO (004), SEM images, and AFM images of surface topography, table of lattice mismatch strain, and polarization *versus* electric field hysteresis loops. This material is available free of charge *via* the Internet at http://pubs.acs.org.

REFERENCES AND NOTES

1. Eerenstein, W.; Mathur, N. D.; Scott, J. F. Multiferroic and Magnetoelectric Materials. *Nature* **2006**, *442*, 759–765.
2. Hill, N. A. Why Are There So Few Magnetic Ferroelectrics. *J. Phys. Chem. B* **2000**, *104*, 6694–6709.
3. Nan, C. W.; Bichurin, M. I.; Dong, S. X.; Viehland, D.; Srinivasan, G. Multiferroic Magnetoelectric Composites: Historical Perspective, Status, and Future Directions. *J. Appl. Phys.* **2008**, *103*, 031101.
4. Nan, C. W.; Liu, G.; Lin, Y. H.; Chen, H. D. Magnetic-Field-Induced Electric Polarization in Multiferroic Nanostructures. *Phys. Rev. Lett.* **2005**, *94*, 197203.
5. Zheng, H.; Wang, J.; Lofland, S. E.; Ma, Z.; Mohaddes-Ardabili, L.; Zhao, T.; Salamanca-Riba, L.; Shinde, S. R.; Ogale, S. B.; Bai, F.; *et al.* Multiferroic $BaTiO_3$−$CoFe_2O_4$ Nanostructures. *Science* **2004**, *303*, 661–663.
6. Newnham, R. E.; Skinner, D. P.; Cross, L. E. Connectivity and Piezoelectric−Pyroelectric Composites. *Mater. Res. Bull.* **1978**, *13*, 525–536.
7. Zavaliche, F.; Zheng, H.; Mohaddes-Ardabili, L.; Yang, S. Y.; Zhan, Q.; Shafer, P.; Reilly, E.; Chopdekar, R.; Jia, Y.; Wright, P.; Schlom, D. G.; *et al.* Electric Field-Induced Magnetization Switching in Epitaxial Columnar Nanostructures. *Nano Lett.* **2005**, *5*, 1793–1796.
8. Zavaliche, F.; Zhao, T.; Zheng, H.; Straub, F.; Cruz, M. P.; Yang, P. L.; Hao, D.; Ramesh, R. Electrically Assisted Magnetic Recording in Multiferroic Nanostructures. *Nano Lett.* **2007**, *7*, 1586–1590.
9. Zheng, H.; Zhan, Q.; Zavaliche, F.; Sherburne, M.; Straub, F.; Cruz, M. P.; Chen, L. Q.; Dahmen, U.; Ramesh, R. Controlling Self-Assembled Perovskite-Spinel Nanostructures. *Nano Lett.* **2006**, *6*, 1401–1407.
10. Ren, S. Q.; Briber, R. M.; Wuttig, M. Diblock Copolymer Based Self-Assembled Nanomagnetoelectric. *Appl. Phys. Lett.* **2008**, *93*, 173507.
11. Levin, I.; Li, J. H.; Slutsker, J.; Roytburd, A. L. Design of Self-Assembled Multiferroic Nanostructures in Epitaxial Films. *Adv. Mater. (Weinheim, Ger.)* **2006**, *18*, 2044–2047.
12. Roy, R. Ceramics by the Solution-Sol−Gel Route. *Science* **1987**, *238*, 1664–1669.
13. Lange, F. F. Chemical Solution Routes to Single-Crystal Thin Films. *Science* **1996**, *273*, 903–909.
14. Gutierrez, J.; Llordes, A.; Gazquez, J.; Gibert, M.; Roma, N.; Ricart, S.; Pomar, A.; Sandiumenge, F.; Mestres, N.; Puig, T.; *et al.* Strong Isotropic Flux Pinning in Solution-Derived $YBa_2Cu_3O_{7-x}$ Nanocomposite Superconductor Films. *Nat. Mater.* **2007**, *6*, 367–373.
15. Ren, S.; Wuttig, M. Spinodally Synthesized Magnetoelectric. *Appl. Phys. Lett.* **2007**, *91*, 083501.
16. Wan, J. G.; Wang, X. W.; Wu, Y. J.; Zeng, M.; Wang, Y.; Jiang, H.; Zhou, W. Q.; Wang, G. H.; Liu, J. M. Magnetoelectric $CoFe_2O_4$-Pb(Zr, Ti)O_3 Composite Thin Films Derived by a Sol−Gel Process. *Appl. Phys. Lett.* **2005**, *86*, 122501.
17. Liu, M.; Li, X.; Lou, J.; Zheng, S. J.; Du, K.; Sun, N. X. A Modified Sol-Gel Process for Multiferroic Nanocomposite Films. *J. Appl. Phys.* **2007**, *102*, 083911.
18. Blamire, M. G.; MaCmanus-Driscoll, J. L.; Mathur, N. D.; Barber, Z. H. The Materials Science of Functional Oxide Thin Films. *Adv. Mater. (Weinheim, Ger.)* **2009**, *21*, 3827–3839.

19. Ahn, K. H.; Lookman, T.; Bishop, A. R. Strain-Induced Metal-Insulator Phase Coexistence in Perovskite Manganites. *Nature* **2004**, *428*, 401–404.
20. Cao, J.; Ertekin, E.; Srinivasan, V.; Fan, W.; Huang, S.; Zheng, H.; Yim, J. W. L.; Khanal, D. R.; Ogletree, D. F.; Wu, J. Strain Engineering and One-Dimensional Organization of Metal-Insulator Domains in Single-Crystal Vanadium Dioxide Beams. *Nat. Nanotechnol.* **2009**, *4*, 732.
21. Lee, M. K.; Nath, T. K.; Eom, C. B.; Smoak, M. C.; Tsui, F. Strain Modification of Epitaxial Perovskite Oxide Thin Films Using Structural Transitions of Ferroelectric $BaTiO_3$ Substrate. *Appl. Phys. Lett.* **2000**, *77*, 3547–3549.
22. Eerenstein, W.; Wiora, M.; Prieto, J. L.; Scott, J. F.; Mathur, N. D. Giant Sharp and Persistent Converse Magnetoelectric Effects in Multiferroic Epitaxial Heterostructures. *Nat. Mater.* **2007**, *6*, 348–351.
23. Tian, H. F.; Qu, T. L.; Luo, L. B.; Yang, J. J.; Guo, S. M.; Zhang, H. Y.; Zhao, Y. G.; Li, J. Q. Strain Induced Magnetoelectric Coupling Between Magnetite and $BaTiO_3$. *Appl. Phys. Lett.* **2008**, *92*, 063507.
24. Czeschka, F. D.; Geprags, S.; Opel, M.; Goennenwein, S. T. B.; Gross, R. Giant Magnetic Anisotropy Changes in Sr_2CrReO_6 Thin Films on $BaTiO_3$. *Appl. Phys. Lett.* **2009**, *95*, 062508.
25. Hayashi, T.; Ohji, N.; Hirohara, K.; Fukunaga, T.; Maiwa, H. Preparation and Properties of Ferroelectric $BaTiO_3$ Thin Films by Sol−Gel Process. *Jpn. J. Appl. Phys., Part 1* **1993**, *32*, 4092–4094.
26. Huang, W.; Zhou, L. X.; Zeng, H. Z.; Wei, X. H.; Zhu, J.; Zhang, Y.; Li, Y. R. Epitaxial Growth of the $CoFe_2O_4$ Film on $SrTiO_3$ and Its Characterization. *J. Cryst. Growth* **2007**, *300*, 426–430.
27. Tan, Z. P. Formation and Piezoelectricity of Self-Assembled $PbTiO_3$−$CoFe_2O_4$ Nanostrutural Films. Ph.D. Thesis, University of Maryland, 2008.
28. Li, Y. L.; Chen, L. Q. Temperature-Strain Phase Diagram for $BaTiO_3$ Thin Films. *Appl. Phys. Lett.* **2006**, *88*, 072905.
29. Zheng, H.; Wang, J.; Mohaddes-Ardabili, L.; Wuttig, M.; Salamanca-Riba, L.; Schlom, D. G.; Ramesh, R. Three-Dimensional Heteroepitaxy in Self-Assembled $BaTiO_3$−$CoFe_2O_4$ Nanostructures. *Appl. Phys. Lett.* **2004**, *85*, 2035–2037.
30. Vandenbo., J; Terrell, D. R.; Born, R. A. J.; Giller, H. An *in Situ* Grown Eutectic Magnetoelectric Composite Material. Part 1. Composition and Unidirectional Solidification. *J. Mater. Sci.* **1974**, *9*, 1705–1709.
31. Schwartz, R. W. Chemical Solution Deposition of Perovskite Thin Films. *Chem. Mater.* **1997**, *9*, 2325–2340.
32. Jia, Q. X.; Mccleskey, T. M.; Burrell, A. K.; Lin, Y.; Collis, G. E.; Wang, H.; Li, A. D. Q.; Foltyn, S. R. Polymer-Assisted Deposition of Metal-Oxide Films. *Nat. Mater.* **2004**, *3*, 529–532.
33. Cullity, B. D.; Graham, C. D. *Introduction to Magnetic Materials,* 2nd ed.; Wiley: Hoboken, N.J., 2005.
34. Luborsky, F. E. High Coercive Materials—Development of Elongated Particle Magnets. *J. Appl. Phys.* **1961**, *32*, S171–S183.
35. Srinivasan, G.; Rasmussen, E. T.; Gallegos, J.; Srinivasan, R.; Bokhan, Y. I.; Laletin, V. M. Magnetoelectric Bilayer and Multilayer Structures of Magnetostrictive and Piezoelectric Oxides. *Phys. Rev. B: Condens. Matter Mater. Phys.* **2001**, *6421*, 214408.
36. Choi, K. J.; Biegalski, M.; Li, Y. L.; Sharan, A.; Schubert, J.; Uecker, R.; Reiche, P.; Chen, Y. B.; Pan, X. Q.; Gopalan, V.; *et al*. Enhancement of Ferroelectricity in Strained $BaTiO_3$ Thin Films. *Science* **2004**, *306*, 1005–1009.
37. Lee, T.; Aksay, I. A. Hierarchical Structure−Ferroelectricity Relationships of Barium Titanate Particles. *Cryst. Growth Des.* **2001**, *1*, 401–419.
38. Scott, J. F. Nanoferroelectrics: Statics and Dynamics. *J. Phys.: Condens. Matter* **2006**, *18*, R361–R386.
39. Schlom, D. G.; Chen, L. Q.; Eom, C. B.; Rabe, K. M.; Streiffer, S. K.; Triscone, J. M. Strain Tuning of Ferroelectric Thin Films. *Annu. Rev. Mater. Res.* **2007**, *37*, 589–626.
40. Pertsev, N. A.; Zembilgotov, A. G.; Tagantsev, A. K. Effect of Mechanical Boundary Conditions on Phase Diagrams of Epitaxial Ferroelectric Thin Films. *Phys. Rev. Lett.* **1998**, *80*, 1988–1991.
41. Rabe, K. M.; Ahn, C. H.; Triscone, J.-M. *Physics of Ferroelectrics: A Modern Perspective;* Springer: Berlin, 2007.
42. Saad, M. M.; Baxter, P.; Bowman, R. M.; Gregg, J. M.; Morrison, F. D.; Scott, J. F. Intrinsic Dielectric Response in Ferroelectric Nanocapacitors. *J. Phys.: Condens. Matter* **2004**, *16*, L451–L456.
43. Chang, L. W.; McMillen, M.; Morrison, F. D.; Scott, J. F.; Gregg, J. M. Size Effects on Thin Film Ferroelectrics: Experiments on Isolated Single Crystal Sheets. *Appl. Phys. Lett.* **2008**, *93*, 132904.
44. Chopdekar, R. V.; Suzuki, Y. Magnetoelectric Coupling in Epitaxial $CoFe_2O_4$ on $BaTiO_3$. *Appl. Phys. Lett.* **2006**, *89*, 182506.
45. Pan, Z. X.; Alem, N.; Sun, T.; Dravid, V. P. Site-Specific Fabrication and Epitaxial Conversion of Functional Oxide Nanodisk Arrays. *Nano Lett.* **2006**, *6*, 2344–2348.